Renewable Energy 180 (2021) 1194–1209

Contents lists available at ScienceDirect

Renewable Energy

journal homepage: www.elsevier.com/locate/renene

Diffuse irradiance on tilted planes in urban environments: Evaluation of models modified with sky and circumsolar view factors

Ignacio García [a, b, *], Marian de Blas [a, b], Begoña Hernández [c, d], Carlos Sáenz [c, d], José Luis Torres [a, b]

[a] Department of Engineering, Public University of Navarre, Campus Arrosadía, 31006, Pamplona, Spain
[b] Institute of Smart Cities (ISC), Public University of Navarre, Campus Arrosadía, 31006, Pamplona, Spain
[c] Department of Science, Public University of Navarre, Campus Arrosadía, 31006, Pamplona, Spain
[d] Institute for Advanced Materials and Mathematics (INAMAT^2), Public University of Navarre, Campus Arrosadía, 31006, Pamplona, Spain

ARTICLE INFO

Article history:
Received 4 June 2021
Received in revised form
10 August 2021
Accepted 12 August 2021
Available online 19 August 2021

Keywords:
Diffuse solar irradiance
Tilted planes
Urban environments
Urban canyon

ABSTRACT

Numerous studies have analyzed existing irradiance models for estimating sky diffuse irradiance on tilted planes. However, few have evaluated the suitability of these models for estimating irradiance in obstructed environments, specifically considering the effects of obstacles. In this study, three irradiance models —one of them with five variants— for estimating diffuse irradiance on tilted planes located in urban environments were evaluated. All models have been adapted to consider the effect of an urban canyon on the diffuse irradiance received on a tilted plane through the sky view factor and the circumsolar view factor. All the models were evaluated against the diffuse irradiance values obtained by the ISO 15469:2004(E)/CIE S 011/E:2003 angular distribution model. Therefore, it was necessary to determine the standard sky type corresponding to each record of the measurements performed by a sky scanner at the radiometric station of UPNA (Spain). A total of 4,864 scenarios were considered to occur from the combination of different orientations and inclinations of the plane, and different orientations and aspect ratios of the urban canyon. The results revealed that the Perez model considering a 35° half-angle circumsolar region has the best performance, followed by the Perez model considering a 45° half-angle circumsolar region.

Nomenclature

α_c	urban canyon aspect ratio
β_p	plane tilt angle
γ_c	urban canyon azimuth measured from due south, increasing towards south-west
γ_i	azimuth angle of a sky element i measured from due south, increasing towards south-west
γ'_i	azimuth angle relative to the normal of the tilted plane of a sky element i
γ_p	plane azimuth angle measured from due south, increasing towards south-west
γ_s	azimuth angle of the sun measured from due south, increasing towards south-west
Δ	sky brightness parameter
ε	sky clearness parameter
θ_i	zenith angle relative to the zenith of a sky element i
θ'_i	zenith angle relative to the normal of the tilted plane of a sky element i
θ_z	zenith angle of the sun
χ_i	angle between the sun and a sky element i
ω_i	solid angle subtended by a sky element i
a	solid angle subtended by the circumsolar region, weighted by its average incidence on the slope
A_I	anisotropy index
b	solid angle subtended by the circumsolar region, weighted by its average incidence on the horizontal
CVF	circumsolar view factor
f	indicatrix function
F_1	circumsolar brightness coefficient
F_2	horizon brightness coefficient
g	gradation function

* Corresponding author. Department of Engineering, Public University of Navarre, Campus Arrosadía, 31006, Pamplona, Spain.
E-mail address: ignacio.garcia@unavarra.es (I. García).

https://doi.org/10.1016/j.renene.2021.08.042

g_d	horizontal diffuse irradiance relative to zenith
$G_{b,n}$	direct normal irradiance (Wm^{-2})
G_d	horizontal diffuse irradiance (Wm^{-2})
$G_{d,T}$	tilted diffuse irradiance (Wm^{-2})
$G_{d,T,i,irr}$	$G_{d,T}$ value obtained by the irradiance model (Wm^{-2})
$G_{d,T,i,CIE}$	$G_{d,T}$ value obtained by the ISO/CIE model (Wm^{-2})
$\overline{G}_{d,T,CIE}$	average of the $G_{d,T}$ values obtained by the ISO/CIE model (Wm^{-2})
l_i	radiance relative to zenith of a sky element i
L_i	radiance of a sky element i ($Wm^{-2}sr^{-1}$)
M	transformation matrix
n	number of considered values of $G_{d,T}$
$n_{c,h}$	number of sky elements corresponding to the circumsolar region projected onto a obstacle-free horizontal plane
$n_{c,T}$	number of sky elements corresponding to the circumsolar region projected onto a tilted plane
$n_{s,h}$	number of sky elements projected onto an obstacle-free horizontal plane
$n_{s,T}$	number of sky elements projected onto a tilted plane
r_i	projected distance between the centroid of a cell element an the center of the grid
SVF	sky view factor

1. Introduction

Solar energy collectors are often installed on non-horizontal surfaces, such as the inclined planes of photovoltaic modules or thermal panels as well as those of building enclosures, e.g., vertical facades. Notwithstanding, weather stations or satellites provide global radiation data in the horizontal plane. This mismatch between the available radiation data and the data needed for the collectors has led to the development of a number of models for the conversion of global radiation from a horizontal to an inclined plane. Over time, models have incorporated a more detailed physical description of the problem, increasing their complexity and computational demands. Recently, artificial intelligence techniques have been applied to address this problem.

Early first-generation models, according to the classification of Muneer et al. [1], made simple assumptions such as considering all global radiation coming directly from the sun. It was soon proved, though, that the different nature of the direct and diffuse components of the radiation required specific, differentiated approaches.

Many irradiance models on a tilted plane, sometimes called transposition models, that make use of irradiance data from weather stations or satellite estimates, have been developed. In these models, the global irradiance on a tilted plane results from the sum of the direct, diffuse, and reflected irradiance from the ground. The vast majority of the models address the computation of the direct irradiance, which can be regarded as a strictly geometric problem, in the same way. The radiation reflected from the ground also exhibits a similar approach in all models, although there are variations in the treatment of the surface albedo. It is in the calculation of the diffuse component where the differences between models are found. In this sense, it is widely accepted that irradiance models can be classified into two major groups: isotropic and pseudo-isotropic models (Liu and Jordan [2], Koronakis [3], Tian et al. [4], Badescu [5]) and anisotropic models (Temps and Coulson [6], Bugler [7], Klucher [8], Steven and Unsworth [9], Hay and Davies [10], Willmott [11], Ma and Iqbal [12], Skartveit et al. [13], Gueymard [14,15], Perez et al. [16,17], Saluja and Muneer [18], Reindl et al. [19], Muneer [20,21]). In the former, it is assumed that the entire sky dome radiates with the same intensity; in other words, radiance remains constant throughout the sky dome, excluding the solar disk. In the latter, anisotropy is tackled with anisotropy indices that describe the varying radiance within the sky dome. In practice, however, some models only establish a reduced number of differentiated zones of the sky, such as the background, circumsolar or horizon, where the radiance remains uniform despite being different from the others. Others consider a functional dependence of the radiance with the cosine of the zenith angle but retain the azimuthal invariance. A time line of the publication dates of these models is shown in Fig. 1.

The performance of these models have been tested for numerous locations and sky conditions. Table 1 provides a review of some studies that have evaluated both isotropic and anisotropic irradiance models at different locations and with different arrangements of the tilted plane. All these studies show that, although no single model clearly outperforms the others for all locations and sky conditions, anisotropic models generally provide a better fit to experimental data. Among anisotropics, Perez's model [17] is usually well positioned, making it a widely used model that has been incorporated into the algorithms of databases such as Meteonorm [22].

All these models were developed or analyzed under astronomical horizon conditions, without regard of the presence of obstacles that could influence the irradiance on a tilted plane. This is however a key issue concerning solar resources in urban environments. In these environments, it is foreseeable that the initial formulation of these models must be reexamined or that models with a different initial approach have to be devised, focusing especially on the calculation of the diffuse component of the solar irradiance.

In their work on the evaluation of energy production from building-integrated photovoltaic systems in urban environments, Costanzo et al. [57] pointed out that irradiance methods for estimating radiation on a tilted plane fail to take into account the obstruction of solar radiation by obstacles or nearby buildings. Taking obstacles into account can be easily done in case of the direct component of the solar radiation, simply setting the direct irradiance to zero when the obstacle blocks the solar disk from view. It is the diffuse component that requires a more sophisticated approach. As a first approximation, assuming that the diffuse sky irradiance on the horizontal plane comes from the whole visible hemisphere, it is possible to consider only the proportion of this hemisphere that is clearly visible from the collection plane, discounting the part hidden by obstacles. This is traditionally evaluated using the sky view factor (*SVF*) [58,59] like in Redweik et al. [60] that used the *SVF* to determine the diffuse irradiance on facades and roofs in an urban environment. They considered the diffuse irradiance to be the result of the integration of radiances from 1,081 non-uniformly distributed radiation sources, adopting the proposal of Ratti and Richens [61]. Here, the authors assumed that sky radiance was isotropic. However, the use of such a strictly geometric *SVF* does not take into account that sky radiance actually has an anisotropic character, with values that can significantly vary between nearby points, depending on the sky conditions.

A different approach would be to integrate the radiance contributions from the different points of the sky dome. This requires the knowledge of the angular distribution of radiance that can be recorded experimentally by means of sky scanners, which are uncommon equipment in weather stations, or estimated with existing angular distribution models.

With regard to the use of sky scanners, it was pointed out in Kómar and Kocifaj [62] that for the estimation of illuminance on vertical surfaces, the field of view should be less than 10°. Gracia et al. [63] compared four models with similar results for all of them. Vartiainen [64] compared the results obtained by five irradiance models and six radiance models with measurements made in an

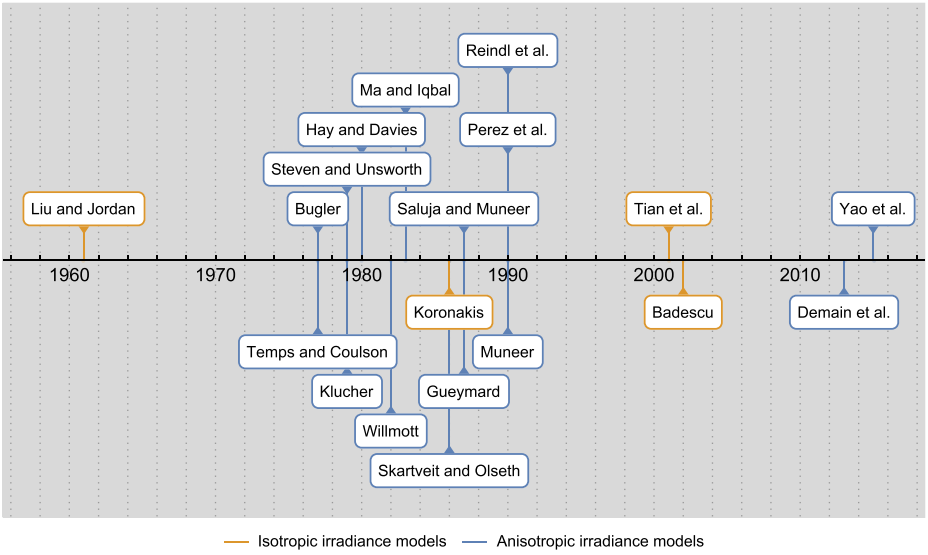

Fig. 1. Timeline of the publication dates of the main irradiance models.

Table 1
Summary of irradiance model evaluation studies.

Study and Location/s	Evaluated Irradiance models	Plane's azimuth and tilt angle	Best performing model/s
Soga et al. [23] Sapporo, Tokyo, and Fukuoka (Japan)	Isotropic: [24]. Anisotropic: [17], [19], [25], [26], [27, 28].	Vertical planes facing N, S, E, W.	Perez et al. [17]
Notton et al. [29] Ajaccio (France)	Isotropic: [2], [3], [30]. Anisotropic: [6], [7], [8], [11], [12], [13], [14, 15], [16, 17, 31], [19], [20, 21], [25], [32].	0°, 45°, and 60° tilted planes. Planes' azimuth not specified.	Perez et al. [31, 16, 17], Ma and Iqbal [12], Klucher [8], Hay [25], Willmott [11], and Skartveit et al. [13].
Gueymard [33] Golden (USA)	Isotropic (source not specified). Anisotropic: [1], [8], [13], [15, 34], [17], [19], [35], [36], [37].	40° tilted plane facing south. 90° tilted plane facing N, S, E, W. 2-axis sun tracking plane.	Gueymard [15, 34] and Perez et al. [17].
Noorian et al. [38] Karaj (Iran)	Isotropic: [2], [3], [4], [5]. Anisotropic: [6], [8], [13], [16], [17], [19], [35], [39].	South-facing plane tilted at 45° and west-facing tilted at 40°.	South-facing planes: Reindl et al. [19], Hay [35], Skartveit et al. [13], and Perez et al. [17]. West-facing planes: Perez et al. [17].
Evseev and Kudish [40] Beer Sheva (Israel)	Isotropic: [2]. Anisotropic: [6], [8], [11], [12], [13], [15, 34], [19], [25], [31, 17], [41].	South-oriented plane tilted at 40°.	Clear and partly cloudy skies: Ma and Iqbal [12]. Overcast skies: Muneer [41].
Khalil and Shaffie [42] Cairo (Egypt)	Isotropic: [2], [3], [4], [5]. Anisotropic: [6], [8], [13], [16], [17], [19], [35], [39].	South-oriented planes tilted at 0°, 15°, 30°, 45°, 60°, 75°, and 90°.	South-facing planes: Perez et al. [17], Hay [35], and Skartveit et al. [13]. West-facing planes: Hay [35] and Perez et al. [17].
Demain et al. [43] Uccle (Belgium)	Isotropic: [2], [3], [5]. Anisotropic: [6], [7], [11], [12], [13], [15], [16], [19], [25], [41].	South-oriented plane tilted at 50.79°.	Bugler [7] but proposed a new coupled model combining Perez et al. [16], Bugler [7], and Willmott [11] models.
Yao et al. [44] Shanghai (China)	Isotropic: [24]. Anisotropic: [1], [6], [8], [13], [15], [17], [19], [35], [44].	30°,45°,60° and 90° tilted planes facing N, S, E, W.	Perez et al. [17] and NADR [44].
Mubarak et al. [45] Hannover (Germany) and Golden (USA)	Isotropic: [2]. Anisotropic: [8], [10], [17], [19].	Hannover: 90° tilted planes facing N, S, E, W, SE, and SW and planes facing south tilted at 0°, 10°, 20°, 30°, 40°, 50°, 60°, 70°. Golden: 40° tilted plane facing south and vertically tilted planes facing N, S, E, W.	Sunny locations: Perez et al. [17]. South-facing tilted planes under cloudy skies: Hay and Davies [10] and Reindl et al. [19].
de Simón-Martín et al. [46] Burgos (Spain) (*)	Isotropic: [2], [3], [4], [5]. Anisotropic: [6], [8], [11], [12], [13], [15, 47], [16, 17], [19], [39], [48], [49], [50], [51, 20], [52], [53, 54, 55].	Vertical planes facing N, S, E, W.	Artificial intelligence models and Perez et al. [17], with locally calibrated coefficients.
García et al. [56] Pamplona (Spain)	Isotropic: [2], [3], [4], [5]. Anisotropic: [1], [6], [7], [8], [9, 39], [10], [11], [12], [15], [16], [17], [19], [43], [44], [53, 55].	26°, 42°, 64° and 90° tilted planes facing N, E, S, W	Perez et al. [17]

(*) de Simón-Martín et al. [46] also evaluated 6 angular radiance distribution models and 4 artificial intelligence models.

open environment in Turku (Finland). Radiance models are more complex than irradiance models due to they consider the angular distribution of radiance in the sky vault. Therefore, the estimation of tilted diffuse irradiance requires the integration, on the tilted plane, of the radiance values corresponding to the sky elements visible from such surface. It was found that the All-weather [65] model had the best performance, being the only radiance model that showed a significant reduction in *RMSE* compared with the Perez et al. [31] model, which was the best among the irradiance models.

To estimate the diffuse irradiance on vertical surfaces in the presence of obstacles and under anisotropic sky conditions, Ivanova [66] proposed a modification of Muneer's irradiance model [21] for surfaces under clear skies. They defined the anisotropic background *SVF* (*ABSVF*) to include the dependence of the sky background radiance with the zenith angle, following the proposal of Steven and Unsworth [39]. They however still considered the circumsolar radiation as coming from a single point. One of these procedures was used by Clarke et al. [67] in their model for estimating the radiation on a tilted plane, called the sky radiance distribution model (SRDM). In this model, the radiance of each of the 145 patches into which the sky dome was divided, was estimated using Perez et al. [17] resulting that the SRDM's *RMSE* was 11% lower than that of Muneer's model.

Recently, Ivanova and Gueymard [68] modeled the anisotropic radiance in open and urban environments using the All-sky model for luminance and radiance from Igawa [69], including the interaction of obstacles with direct and diffuse radiation through an orthographic projection of the whole sky dome. The authors claimed that the proposed method could be used to generate long time-series of irradiance values in any plane of a complex environment (e.g., urban environment) with greater precision than previous approaches using the isotropic *SVF*. Their proposal has been integrated in an improvement of the existing SOLARES software, which permits different levels of discretization of the sky dome.

In summary, numerous studies have tested existing models for the estimation of the irradiance on tilted planes. However, there are still very few studies concerning model performance in the increasingly interesting case of obstructed environments, specifically with regard to the effect of obstacles on the diffuse component of global irradiance. The authors' research interest focuses on estimating the solar resource on planes located in urban environments. In most of the mentioned, nowadays widely used, irradiance models the treatment of the direct and reflected components of the irradiance received on the tilted plane is exactly the same. The difference between these models lies in the estimation of the diffuse component of the sky irradiance, which can determine their global performance. For this reason, the present work tries to reduce the existing gap of knowledge in the context of diffuse irradiance modeling in urban environments, by evaluating three irradiance models —one of them with five variants— on a tilted plane in obstructed environments. The original formulation of these models was modified to consider the effect of obstructions on the diffuse irradiance received on the tilted plane in a complex environment.

To analyze the behavior of irradiance models when they are faced with urban configurations of varying complexity, the idea of an urban canyon [70] has been used and adopted here as an archetype of the real urban environment. Regardless of the degree of similarity of the urban canyon with a specific urban environment —since the number of possible urban configurations is endless—, the use of this geometric simplification gives a clear insight into the behavior of the models' performance as a function of the level of obstruction of the environment.

The *SVF* has been used to introduce the effect of the urban canyon on the diffuse isotropic background irradiance and the circumsolar view factor (*CVF*) to consider the effect on the circumsolar region. A procedure for calculating the *SVF* and *CVF*, based on the orthographic projection of the sky on the tilted plane of interest is proposed. Taking into account the positions of the plane and the different configurations of the urban canyon, 4,864 scenarios were considered. For each scenario and model, predictions were compared with the reference irradiance provided by the model proposed in the CIE Standard General Sky [71] and obtained from the measured angular distribution of sky radiance in 5,396 different sky conditions comprising the 15 types of ISO/CIE standard skies.

This paper is organized into five sections and two appendices. The meteorological data, the measurement equipment and the quality control procedures are detailed in Section 2. Section 3 describes the general methodology applied. Section 4 presents the results obtained by the evaluated models in the different scenarios as well as their overall ranking scores. The conclusions are detailed in Section 5. The methodology proposed for the projection of the sky radiance distribution onto a generic tilted plane is detailed in Appendix A. Appendix B describes the proposed methodology for the calculation of *SVF* and *CVF*.

2. Meteorological data

The data used in this study were collected from the radiometric station of the UPNA, located on the roof of one of the buildings of the Higher Technical School of Agricultural Engineering and Biosciences (42°47′32″ N, 1°37′45″ W, 435 m a.s.l.) in Pamplona (Spain). The study of the visible horizon revealed that the elevation does not exceed 6° in any direction. The data series consist in 6,767 observations made between July and December 2018. Measured variables include 1-min frequency data of global irradiance on the horizontal plane, using a Kipp & Zonen CM11 pyranometer, diffuse irradiance on the horizontal plane with a Kipp & Zonen CM11 pyranometer with a shadow ball, and direct normal irradiance with a Kipp & Zonen CH1 pyrheliometer. All three instruments were mounted on a Kipp & Zonen 2AP solar tracker. In addition, the angular distribution of sky radiance was measured every 10 min using an EKO MS-321LR sky scanner. This scanning device records the radiance and luminance values of 145, approximately uniformly distributed sky patches according to the CIE recommendation [72].

Both irradiance and angular distribution measurements corresponding to solar elevations below 5° were discarded. Irradiance measurements were further subjected to the quality control procedure proposed by the MESoR project [73]. In the case of angular distribution of radiance, quality control was based in three criteria. First, all measurements of individual sky patches with values outside the measurement range of the sky scanner (0–300 $Wm^{-2}sr^{-1}$) were discarded. Second, all measurements of sky patches whose center was less than 6° from the sun were discarded, since the sun's radiance exceeded the sky scanner's maximum measurable value. Third, all measurements whose integration on the horizontal plane deviated by more than 30% from the diffuse irradiance measured in the same time period were also discarded in accordance with the quality control test applied by Li et al. [74] to radiance and luminance measurements.

3. Methodology

The general methodology consists of: (1) the estimation of the diffuse irradiance on the tilted plane from the measured angular distribution of radiance and the ISO/CIE model, considering the obstruction provided by the urban canyon; (2) obtaining the diffuse

irradiance predicted by each of the irradiance models, modified to include the effect of obstructions on the diffuse component; and (3) the comparison of model predictions with the reference irradiance values given by the ISO/CIE angular distribution model.

This methodology was applied to a total of 4,864 scenarios resulting from the combination of 8 different orientations (γ_p) and 19 inclinations (β_p) of the tilted plane and 4 orientations (γ_c) and 8 aspect ratios (α_c) of the urban canyon, listed in Table 2. The aspect ratio is considered as the quotient of the height and width of the urban canyon, as shown in Fig. 2. A large number of scenarios were considered to cover as many situations as possible that can occur in a real urban environment. For all scenarios, the tilted plane of interest was considered to be in the center of the urban canyon, i.e., equidistant to the two facades that delimit the canyon.

The ISO/CIE angular distribution model was used to obtain the reference diffuse irradiance —against which values provided by the analyzed irradiance models were compared— because of two fundamental reasons. The first is the practical imposibility to install irradiance sensors in such a large number of considered scenarios. The second is to overcome data discontinuities resulting from the saturation of the sky scanner measurements of angular distribution of radiance in those patches close to the sun, as explained in Section 2. The measurements of angular distribution of radiance were used to characterize the state of the sky according to the ISO/CIE standard. In this way, it was possible to determine the theoretical ISO/CIE radiance distribution closest to the real, measured distribution. Then, the model proposed in the standard was used to obtain a continuous distribution of radiance in the sky according to the ISO/CIE sky-type obtained. It could be argued that the ISO/CIE model is designed to describe the luminance distribution of the sky and not the radiance. However García et al. [75] found that classification in sky types from radiance and luminance measurements gives an exact match for nearly 60% of the cases and reaches 90% when, in addition to the matching classifications, the differences of 1 and 2 sky types are considered.

All the models used in this study were programmed in Wolfram Mathematica® and executed in the Computing Cluster of the UPNA Research Institutes.

3.1. Estimation of the diffuse irradiance on the tilted plane by the ISO/CIE angular distribution model

Fig. 3 summarizes the procedure for estimating the diffuse irradiance on the tilted plane from the ISO/CIE angular distribution model. For each record in the data series, the sky type was first classified according to the ISO/CIE standard using the RZL method proposed by García et al. [75]. It is common for some of the skies classified as overcast to show an excessively high direct irradiance on the normal plane ($G_{b,n}$), or for skies classified as clear to show abnormally low values of $G_{b,n}$. These skies are known as *opposite* skies, as opposed to *normal* skies. Following the ISO/CIE classification, we distinguished between *normal* and *opposite* skies according to the criteria of Bartzokas et al. [76], i.e., $G_{b,n} \geq 120\text{Wm}^{-2}$ for sky types 1–6 and $G_{b,n} < 120\text{Wm}^{-2}$ for sky types 7–5. Opposite skies were discarded in this study.

The projection of the radiance relative to the zenith of a series of sky elements was calculated by the ISO/CIE model on the plane of interest, defined by its azimuth and tilt angles. For this purpose, a grid consisting of 1000 × 1000 square cells located on the tilted plane was considered. Each of these cells corresponds to the orthographic projection of a sky element onto that plane. Since the orthographic projection of the entire sky vault corresponds to a circle, only 782,268 grid cells enclosed by that circle are effective calculation cells. The procedure used to project the radiance relative to the zenith onto the inclined plane, for a given sky element, is detailed in Appendix A.

Table 2
Considered configurations of the urban canyon and tilted plane.

Variable	Initial value	Final value	Increment	Cases
Urban canyon azimuth (γ_c)	0°	135°	45°	4
Urban canyon aspect ratio (α_c)	0.5	4	0.5	8
Plane tilt angle (β_p)	0°	90°	5°	19
Plane azimuth (γ_p)	−180°	135°	45°	8

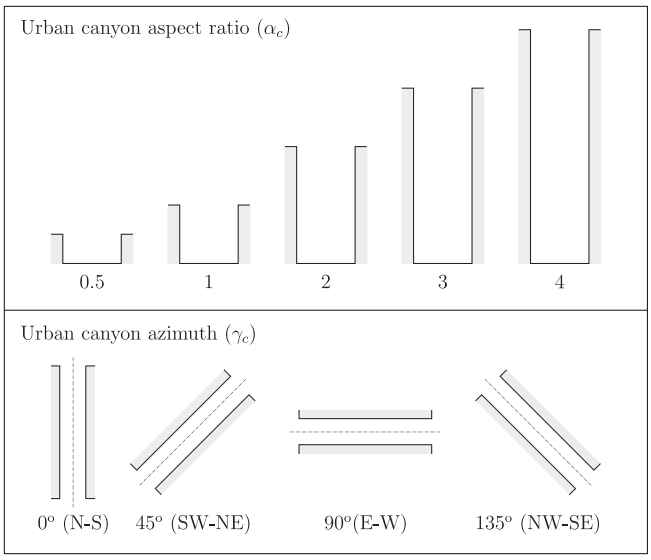

Fig. 2. Definition of the geometry (α_c) and orientation (γ_c) of the urban canyon.

The projection of the absolute radiance distribution onto the tilted plane can be obtained by multiplying the relative radiance calculated for each cell of the grid by the zenith radiance. To ensure the consistency between the angular distribution of absolute radiance and the integrated, measured diffuse irradiance on the horizontal plane, the multiplicative factor was obtained according to the following procedure (see Fig. 3):

1. Calculation of the projection onto the horizontal plane of the angular distribution of the radiance relative to the zenith corresponding to the obtained ISO/CIE sky type.
2. Obtaining the horizontal diffuse irradiance relative to the zenith (g_d) as the sum of the calculated relative radiance values (l_i) corresponding to the sky elements projected onto the horizontal plane, according to Equation (1).

$$g_d = \sum_{i=1}^{N} l_i \cos(\theta_i')\omega_i, \tag{1}$$

where ω_i is the solid angle subtended by the sky element i, as seen from the tilted plane. The summation extends to the N grid cells corresponding to the effective calculation cells, excluding those cells within the 2.5° region around the sun's position that was obstructed by the shadow ball used in the measurement of the diffuse irradiance on the horizontal plane.

Because an orthographic projection is used, the product of $\cos(\theta_i')\omega_i$ is simply a constant k. Therefore, Equation (1) can be rewritten as Equation (2) with g_d equal to the product of the

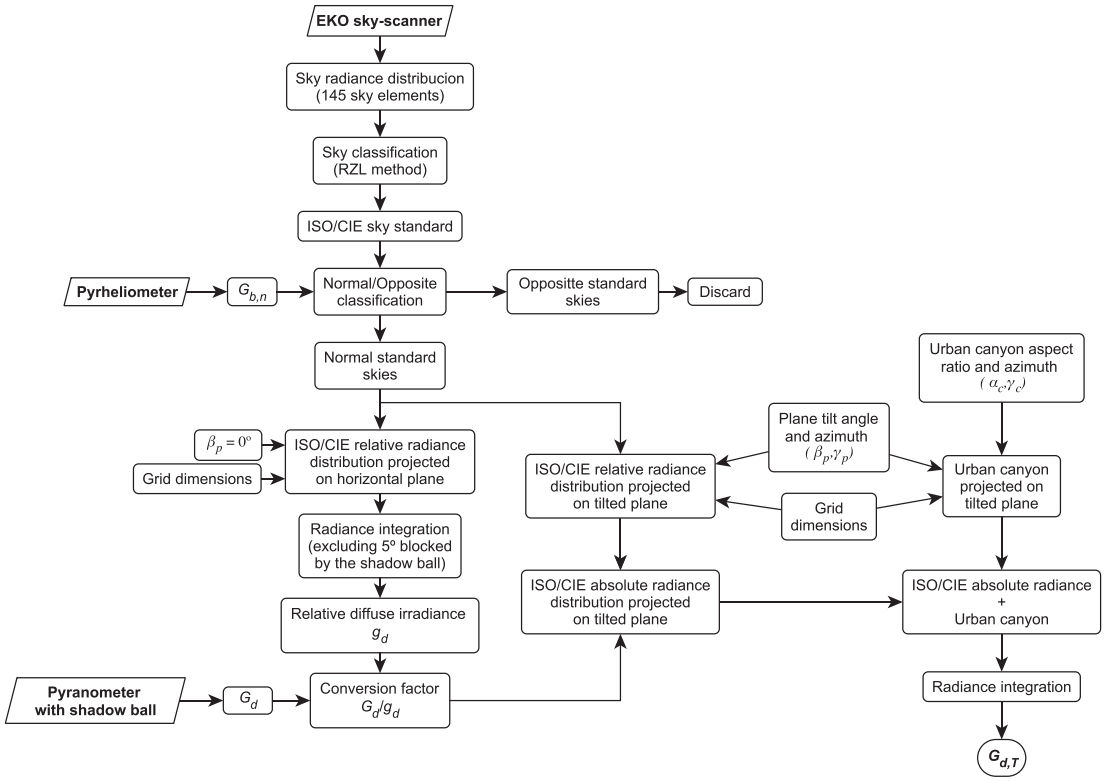

Fig. 3. Methodology for the estimation of diffuse irradiance on the tilted plane using the ISO/CIE model.

constant k times the sum of the relative radiance l_i of the N sky elements visible from the tilted plane.

$$g_d = k\sum_{i=1}^{N} l_i. \tag{2}$$

3. Obtaining the conversion factor by the quotient of the G_d measured by the pyranometer with a shadow ball, and the calculated g_d.
4. Determination of the absolute radiance values corresponding to the projection of the grid sky elements onto the inclined plane as the product of the conversion factor and the relative radiance values.

At this point, the integration of the angular distribution values of absolute radiance projected onto the tilted plane would correspond to the diffuse irradiance values on the inclined plane in an obstacle-free environment. However, the objective of this study is to evaluate the behavior of irradiance models in the presence of obstacles. To take into account the effect of the urban canyon on the diffuse irradiance on an inclined plane placed inside it, those sky elements hidden from view by the urban canyon must be eliminated from the summation. For this, a procedure similar to that described in Appendix A was followed. That is, the urban canyon was projected onto the tilted plane according to the defined grid. In this case, grid cells take the value 1 if the centroid of the sky element is visible from the tilted plane, and 0 if it is obstructed by the urban canyon. Finally, the values of the absolute radiance grid and those of the sky visibility grid were multiplied element by element. The sum of the resulting grid values corresponds to the incident diffuse irradiance on an inclined plane inside the urban canyon. As an example, Fig. 4 shows the projection of the angular distribution of radiance corresponding to the ISO/CIE sky standard 7 onto an obstacle-free tilted plane (Fig. 4a), as well as the projection of five urban canyons with different aspect ratios (Fig. 4b to f).

3.2. Estimation of diffuse irradiance on the inclined plane by the modified irradiance models

The evaluated models for estimating the diffuse irradiance on an inclined plane, modified for obstructed environments, are listed in Table 3. Model selection, from among those cited in Section 1, was based on the possibility of integrating into their formulation the effect of the urban canyon or any other type of obstruction on the diffuse irradiance on a tilted plane. Studied models include an isotropic sky model (i.e., the Liu and Jordan [2] model), and six anisotropic sky models including the Hay and Davies [10] model, with a point source circumsolar region, and five variants of the Perez et al. [16] model. The five variants of the Perez model differ in the aperture angle of the circumsolar region. In particular, aperture angles in Perez et al. [16] (point source, 15°, 25° and 35°) as well as an additional 45° half-angle circumsolar region have been considered. In Perez's models coefficients from Perez et al. [17] were used in case of the point-source circumsolar model and coefficients from Perez et al. [16] in the case of non-pointlike circumsolar region. Likewise, as can be seen in Section 1, the Perez model is one of best performing irradiance models in the model evaluations carried out so far.

In their original formulation, all these models take into account the effect of the inclination of the plane on the received irradiance, without regard of possible obstructions. In consequence, they must be modified in order to consider the effect of the urban canyon. This has been done by means of two view factors. Specifically, the isotropic component of these models was modified through the *SVF*, the ratio of the diffuse irradiance on a tilted plane and on a

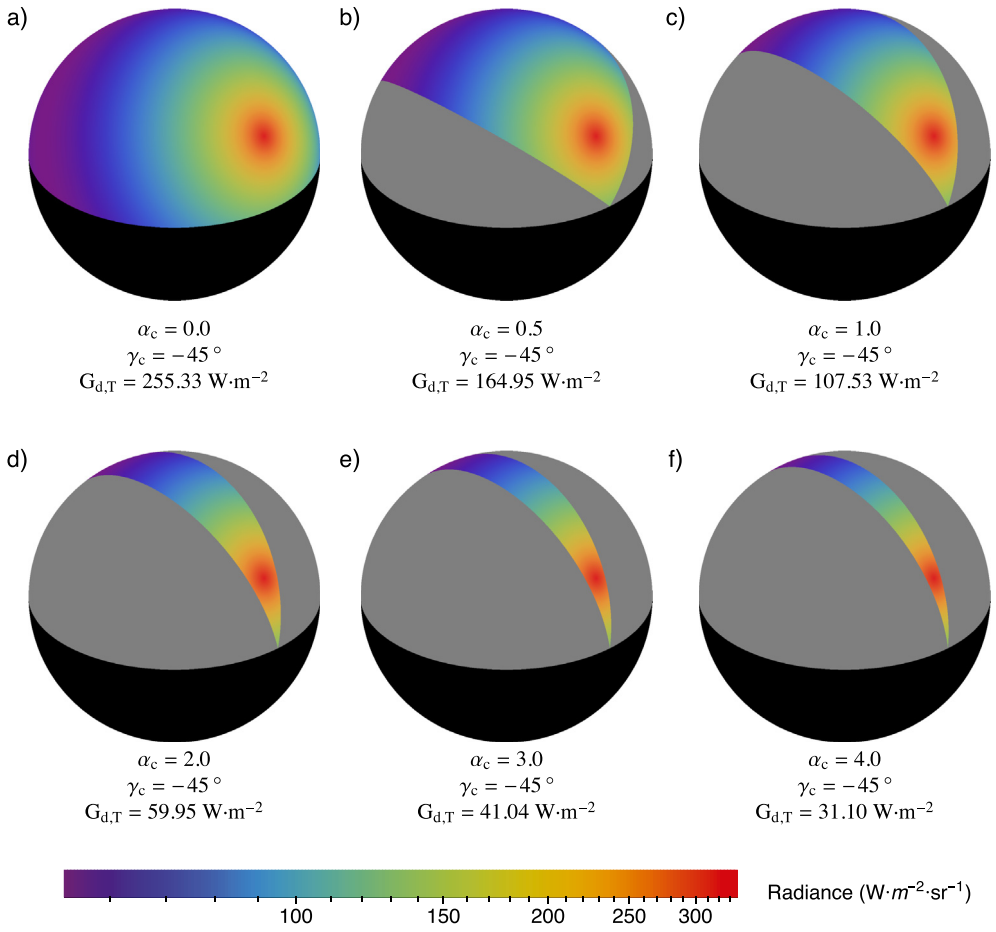

Fig. 4. Projection of the ISO/CIE sky standard 7 onto a plane with an inclination $\beta_p = 60°$ and an azimuth $\gamma_p = -45°$, located in the center of the urban canyon, when the sun has a solar zenith angle $\theta_z = 60°$ and a solar azimuth $\gamma_s = -45°$, considering different aspect ratios of the urban canyon. The diffuse irradiance on the inclined plane ($G_{d,T}$) is included at the bottom of each figure. The black-shaded area corresponds to the visible part of the ground as a consequence of the inclination of the plane. The gray-shaded area corresponds to the projection of the urban canyon onto the tilted plane.

Table 3
Evaluated irradiance models.

Model	Model type	Reference	Year	Circumsolar region half-angle (°)
Liu–Jordan	Isotropic	Liu and Jordan [2]	1961	No
Hay–Davies	Anisotropic	Hay and Davies [10]	1980	Point source
Perez1	Anisotropic	Perez et al. [17]	1990	Point source
Perez2	Anisotropic	Perez et al. [16]	1987	15°
Perez3	Anisotropic	Perez et al. [16]	1987	25°
Perez4	Anisotropic	Perez et al. [16]	1987	35°
Perez5	Anisotropic	Perez et al. [16]	1987	45°

horizontal plane for an isotropic distribution of the sky radiance. The *CVF*, the ratio of the circumsolar irradiance received on a tilted plane and on a horizontal plane, was used to include the effect of obstacles in those models including an explicit term for the circumsolar component. In models that consider a point-source circumsolar region the *CVF* cannot be used and the original formulation was retained for this component. The modified version of each model is presented in Sections 3.2.1–3.2.3. A procedure for calculating the *SVF* and *CVF* in the presence of obstacles, based on the comparison of the projection of both sky regions onto a horizontal plane and tilted plane of interest, is detailed in Appendix B.

3.2.1. The modified Liu–Jordan model

Equation (3) shows the original formulation of the Liu and Jordan [2] model for calculating $G_{d,T}$ considering an isotropic distribution of sky radiance.

$$G_{d,T} = G_d\left(\frac{1+\cos\beta_p}{2}\right) \tag{3}$$

In the modified version proposed in this paper, Equation (4), the factor $\left(1+\cos\beta_p\right)/2$ is replaced by the *SVF* value corresponding to each plane arrangement and the characteristics of the urban canyon.

$$G_{d,T} = G_d SVF. \tag{4}$$

3.2.2. The modified Hay–Davies model

This model considers the irradiance coming from the isotropic background and from a pointlike circumsolar region concentrated at the sun's position. The original version of the Hay and Davies [10] model is shown in Equation (5).

$$G_{d,T} = G_d\left[(1-A_I)\left(\frac{1+\cos\beta_p}{2}\right)+A_I\frac{\cos\iota}{\cos\theta_z}\right], \quad (5)$$

where the anisotropy index A_I is the ratio between $G_{b,n}$ and the normal extraterrestrial irradiance ($G_{0,n}$)

As in the preceding model, in our modified version, Equation (6), the factor $\left(1+\cos\beta_p\right)/2$ is replaced by the *SVF*.

$$G_{d,T} = G_d\left[(1-A_I)SVF+A_I\frac{\cos\iota}{\cos\theta_z}\right] \quad (6)$$

3.2.3. The modified Perez model

The original model published by Perez et al. [16] is shown in Equation (7). The three terms in this equation correspond to the diffuse irradiance from the isotropic background region, the circumsolar region and the contribution of the horizon brightness.

$$G_{d,T} = G_d\left[(1-F_1)\left(\frac{1+\cos\beta_p}{2}\right)+F_1\frac{a}{b}+F_2\sin\beta_p\right], \quad (7)$$

where F_1 is the circumsolar brightness coefficient; F_2 is the horizon brightness coefficient; a is the solid angle subtended by the circumsolar region, weighted by its average incidence on the slope; and b is the solid angle subtended by the circumsolar region, weighted by its average incidence on the horizontal. Coefficients F_1 and F_2 depend on two parameters used to characterize the sky conditions at a given time: sky clearness (ε) and sky brightness (Δ).

In our proposal, the first term, the contribution of the isotropic background, is modified exactly as in the previous models, replacing the factor $\left(1+\cos\beta_p\right)/2$ by the *SVF*. In the case of the circumsolar component, the factor a/b is replaced by the *CVF*. Finally, the term related to the horizon brightness is eliminated, in the understanding that this sky region will be obstructed, almost completely, by the urban canyon. Therefore, the modified Perez model is given by Equation (8).

$$G_{d,T} = G_d[(1-F_1)SVF+F_1CVF] \quad (8)$$

4. Results and discussion

4.1. Sky classification according to ISO/CIE standard

After the application of the RZL sky classification method, it was observed that the *opposite* skies accounted for 19.91% of sky types 1–6 and 8.65% of sky types 7–15. *Opposite* skies were discarded and, out of the 6,767 measurements initially recorded, the remaining 5,396 *normal* skies conformed the data set used in this study. Within this data set, the frequency of occurrence of each ISO/CIE sky type is shown in Fig. 5. During the studied period of time, 24.81% overcast skies (types 1–5), 19.14% intermediate skies (types 6–10), and 56.04% clear skies (types 11–15) were observed.

4.2. Evaluation of modified irradiance models

For each record in the data set, once the ISO/CIE sky type was identified, the diffuse irradiance on the tilted plane was determined by the ISO/CIE radiance angular distribution model for each of the 4,864 scenarios considered. These irradiance values were used as the reference against which the irradiance estimates provided by the modified irradiance models described in Sections 3.2.1–3.2.3 were compared. For each scenario and modified model, the performance was evaluated with the *rRMSE*, according to Equation (9).

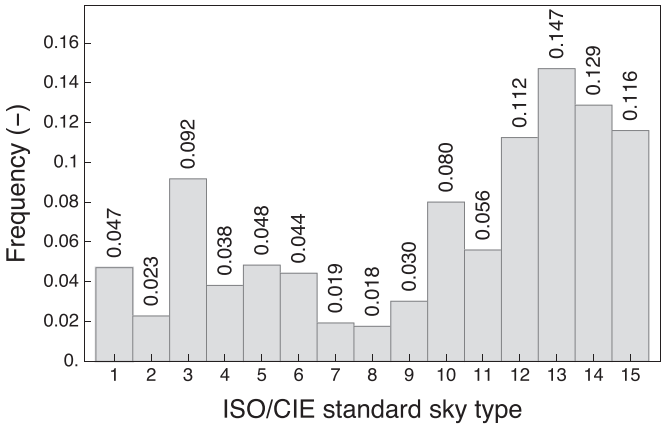

Fig. 5. Observed frequency of occurrence of each sky type in the dataset, according to the CIE Standard General Sky classification [71].

$$rRMSE(\%) = \frac{100}{G_{d,T,CIE}}\sqrt{\frac{\sum_{i=1}^{n}\left(G_{d,T,i,CIE}-G_{d,T,i,irr}\right)^2}{n}}, \quad (9)$$

where the summation extends to the n = 5,396 *normal* skies in the data set and, for each scenario i, $G_{d,T,i,CIE}$ is the diffuse irradiance on the tilted plane calculated from the ISO/CIE angular radiance distribution model and $G_{d,T,i,irr}$ is the diffuse irradiance on the tilted plane given by the modified irradiance model. Finally $\bar{G}_{d,T,CIE}$ is the average value of $G_{d,T,i,CIE}$ over the n scenarios.

As an example, Fig. 6 shows the errors obtained by each irradiance model for particular orientations of the inclined plane ($\gamma_p = -90°$) and of the urban canyon ($\gamma_c = 135°$, NW-SE). Each graph in Fig. 6 shows, for a given model, a two dimensional contour plot of the *rRMSE* values as a function of the plane tilt angle (β_p) and canyon aspect ratio (α_c). In the example shown in Fig. 6 *rRMSE* increases with α_c and β_p. This effect is most evident in the two models that consider a point-source circumsolar region (Hay–Davies and Perez1), where *rRMSE* values reached 200%. The Perez4 model obtained the lowest errors. The isotropic sky model (Liu–Jordan) showed a good performance, better than that of anisotropic models that consider a point-source circumsolar region.

Fig. 7 shows an analogous example to that depicted in Fig. 6, in this case for a $\gamma_p = -90°$ and a $\gamma_c = 135°$ (NE-SW). A different pattern is shown here than in the previous example, which is particularly noticeable in the Hay–Davies and Perez1 models. In these cases, the highest *rRMSE* values are found for plane tilt angles close to 0° and high values of α_c.

Similar plots, not shown here owing to space limitations, have been constructed for the other 30 combinations of γ_p and γ_c. Several trends can be identified in the qualitative and quantitative analysis of these plots. In particular, there are two features that can be linked to the sky data set. Firstly, plots corresponding to pairs of scenarios with orientations that are symmetric with respect to the N–S axis, for instance the scenario with $\gamma_p = -45°$ and $\gamma_c = 0°$ and the scenario with $\gamma_p = 45°$ and $\gamma_c = 0°$, are almost identical.

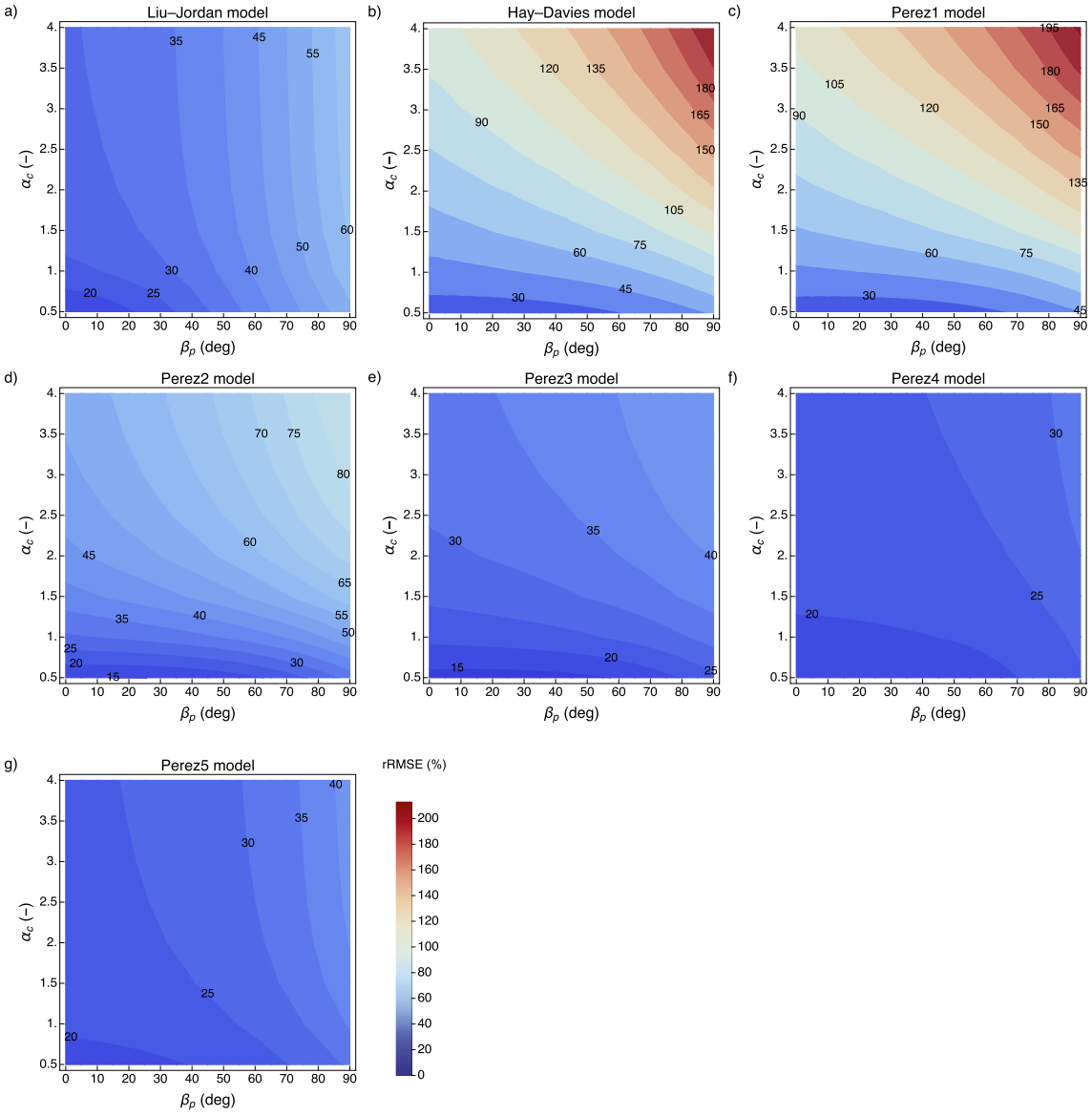

Fig. 6. *rRMSE* (%) values of tilted diffuse irradiance obtained by each model for the different β_p and α_c combinations considering a γ_p of − 90° and a γ_c of 135° (NW-SE).

Actually, this is the expected result for a statistically representative sample of all possible sun's azimuths and sky conditions and it can be regarded as a confirmation that our data set is not biased in azimuth. Secondly, it is found that, independently of the urban canyon orientation and of the particular model, *rRMSE* values tend to increase with increasing tilt angles (β_p) for southern oriented planes (γ_p = 0°, − 45°, 45°). Conversely, *rRMSE* values tend to decrease with increasing tilt angles for northern oriented planes ($\gamma_p = -180°, -135°, 135°$). This behavior is clearly a consequence of the site latitude (42°47′32″ N), where the sun's daily path is mainly constrained within southern azimuths ($-90° \leq \gamma_s \leq 90°$). Finally, a third feature, not connected with the particular site, is the positive correlation between *rRMSE* values and the aspect ratio α_c. Setting aside the evident differences in absolute *rRMSE* values, this positive correlation pertains to all models, canyon orientations and tilt angles. It must be therefore regarded as a genuine effect of the urban canyon characteristics.

Data in those 32 plots like Figs. 6 and 7 can be summarized in a more concise form calculating the abridged *rRMSE* values that take into account, in addition to all sky conditions in the data set, all possible orientations and inclinations of the plane. In this way, model's performance at a given urban canyon orientation (γ_c) and aspect ratio (α_c) can be quantified. The resulting *rRMSE* values are shown in Tables 4–7. Each table corresponds to one of the studied values of γ_c and lists the *rRMSE* values for each model and canyon aspect ratio α_c. For each α_c, models have been ranked according to their *rRMSE* values and their rank order is shown in brackets. It can be seen that Perez4 model (35° half-angle circumsolar region) is

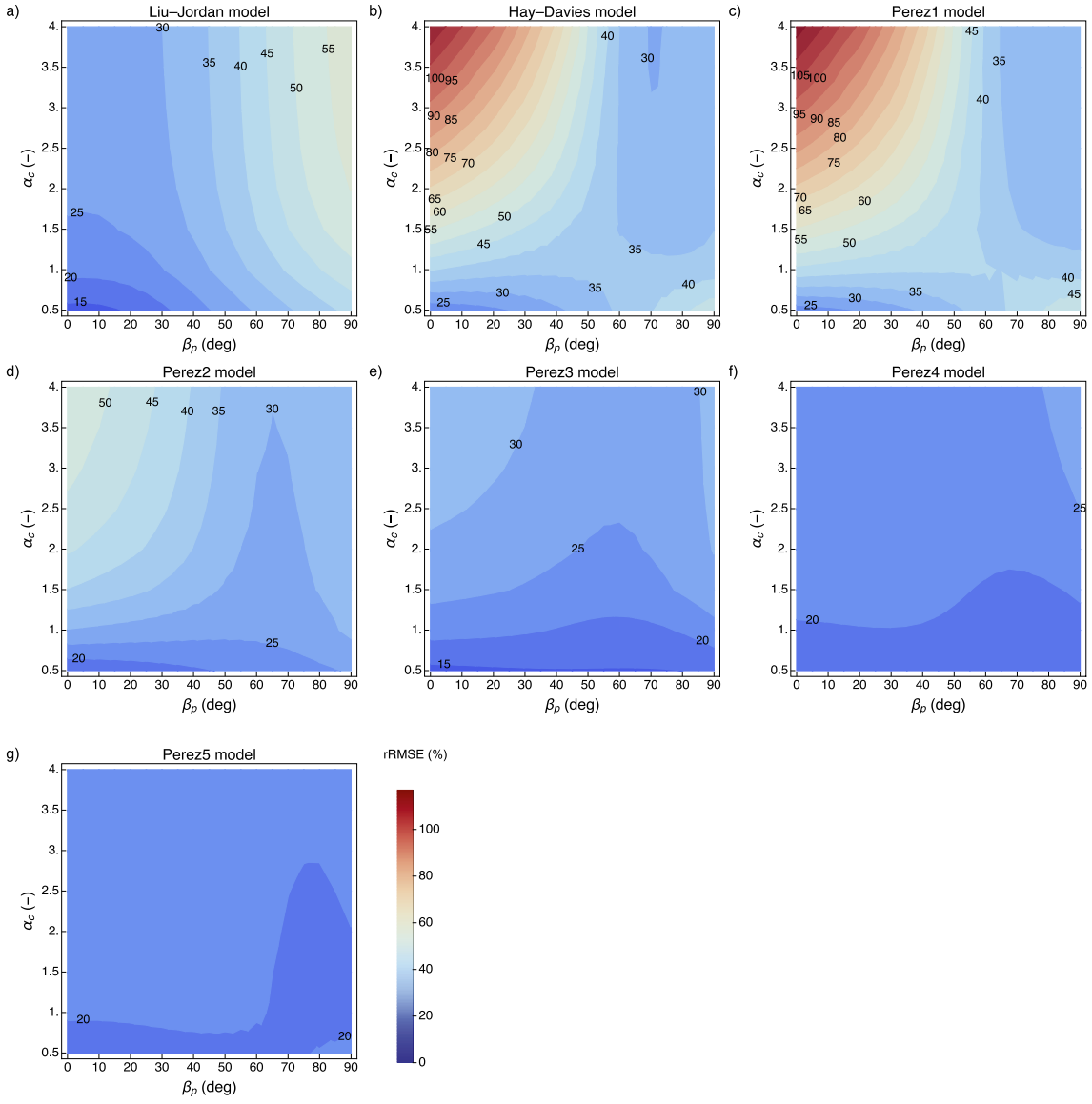

Fig. 7. *rRMSE* (%) values of tilted diffuse irradiance obtained by each model for the different β_p and α_c combinations considering a γ_p of $-90°$ and a γ_c of 45° (NE-SW).

Table 4
rRMSE (%) values of tilted diffuse irradiance obtained by each model for different α_c considering a γ_c of 0° (N–S). For each α_c, model rank scores are shown in parenthesis.

α_c	Liu–Jordan		Hay–Davies		Perez1		Perez2		Perez3		Perez4		Perez5	
0.5	30.25	(7)	29.45	(6)	28.24	(5)	20.15	(3)	16.55	(1)	18.02	(2)	20.82	(4)
1.0	35.15	(5)	45.47	(6)	47.85	(7)	32.96	(4)	23.89	(3)	20.87	(1)	23.42	(2)
1.5	37.28	(4)	60.05	(6)	65.10	(7)	41.88	(5)	27.90	(3)	22.50	(1)	24.74	(2)
2.0	38.27	(4)	74.20	(6)	81.15	(7)	47.52	(5)	30.25	(3)	23.60	(1)	25.52	(2)
2.5	38.78	(4)	85.45	(6)	94.25	(7)	51.14	(5)	31.71	(3)	24.36	(1)	25.99	(2)
3.0	39.08	(4)	94.82	(6)	105.34	(7)	53.55	(5)	32.70	(3)	24.89	(1)	26.31	(2)
3.5	39.29	(4)	104.49	(6)	116.22	(7)	55.25	(5)	33.40	(3)	25.28	(1)	26.55	(2)
4.0	39.41	(4)	111.68	(6)	125.91	(7)	56.36	(5)	33.87	(3)	25.55	(1)	26.70	(2)

the best performing model, except for the particular value $\gamma_c = 90°$, where Perez5 model (45° half-angle circumsolar region) is slightly better. For $\alpha_c = 0.5$, Perez3 model (25° half-angle circumsolar region) is always ranked in first position. In general, the Liu–Jordan model occupies an intermediate position in the classification.

Finally, in line with the work of Yang [77], a linear ranking method [78] was used to classify the models according to their *rRMSE*. From the partial classifications corresponding to each scenario, the global classification ($\mathcal{R}_i$) was obtained for each α_c and for the set of all scenarios by Equation (10).

Table 5
rRMSE (%) values of tilted diffuse irradiance obtained by each model for different α_c considering a γ_c of 45° (SW-NE). For each α_c, model rank scores are shown in parenthesis.

α_c	Liu–Jordan		Hay–Davies		Perez1		Perez2		Perez3		Perez4		Perez5	
0.5	28.99	(5)	30.97	(7)	30.31	(6)	20.81	(4)	16.36	(1)	17.79	(2)	20.19	(3)
1.0	32.97	(4)	47.92	(6)	49.82	(7)	33.42	(5)	23.85	(3)	20.52	(1)	22.27	(2)
1.5	34.94	(4)	61.88	(6)	64.54	(7)	42.18	(5)	28.08	(3)	21.74	(1)	23.38	(2)
2.0	35.87	(4)	74.98	(6)	77.98	(7)	47.22	(5)	30.42	(3)	22.68	(1)	24.08	(2)
2.5	36.36	(4)	87.08	(6)	90.21	(7)	50.14	(5)	31.83	(3)	23.39	(1)	24.54	(2)
3.0	36.64	(4)	98.05	(6)	101.17	(7)	52.07	(5)	32.77	(3)	23.94	(1)	24.87	(2)
3.5	36.84	(4)	108.31	(6)	110.85	(7)	53.44	(5)	33.45	(3)	24.36	(1)	25.13	(2)
4.0	36.95	(4)	118.71	(6)	120.41	(7)	54.36	(5)	33.91	(3)	24.67	(1)	25.32	(2)

Table 6
rRMSE (%) values of tilted diffuse irradiance obtained by each model for different α_c considering a γ_c of 90° (E-W). For each α_c, model rank scores are shown in parenthesis.

α_c	Liu–Jordan		Hay–Davies		Perez1		Perez2		Perez3		Perez4		Perez5	
0.5	28.68	(5)	32.23	(7)	31.70	(6)	23.12	(4)	16.63	(1)	17.68	(2)	20.41	(3)
1.0	31.19	(5)	55.71	(6)	58.47	(7)	29.29	(4)	20.61	(3)	20.43	(2)	20.40	(1)
1.5	32.45	(4)	63.26	(6)	65.95	(7)	35.73	(5)	23.83	(3)	21.93	(2)	20.46	(1)
2.0	33.08	(4)	69.72	(6)	71.29	(7)	40.59	(5)	26.73	(3)	22.98	(2)	21.00	(1)
2.5	33.43	(4)	76.04	(6)	77.18	(7)	43.67	(5)	28.89	(3)	23.66	(2)	21.47	(1)
3.0	33.63	(4)	81.19	(6)	82.38	(7)	45.40	(5)	30.47	(3)	24.17	(2)	21.81	(1)
3.5	33.78	(4)	85.62	(6)	87.22	(7)	46.41	(5)	31.68	(3)	24.60	(2)	22.08	(1)
4.0	33.87	(4)	90.57	(6)	92.44	(7)	47.04	(5)	32.56	(3)	24.93	(2)	22.26	(1)

Table 7
rRMSE (%) values of tilted diffuse irradiance obtained by each model for different α_c considering a γ_c of 135° (NW-SE). For each α_c, model rank scores are shown in parenthesis.

α_c	Liu–Jordan		Hay–Davies		Perez1		Perez2		Perez3		Perez4		Perez5	
0.5	29.22	(5)	30.68	(7)	30.05	(6)	20.55	(3)	16.13	(1)	17.90	(2)	20.63	(4)
1.0	33.88	(5)	45.97	(6)	47.97	(7)	32.82	(4)	23.52	(3)	20.48	(1)	22.77	(2)
1.5	36.10	(4)	59.02	(6)	63.74	(7)	40.59	(5)	27.81	(3)	21.82	(1)	23.79	(2)
2.0	37.13	(4)	69.45	(6)	74.61	(7)	45.29	(5)	30.21	(3)	22.87	(1)	24.46	(2)
2.5	37.66	(4)	79.09	(6)	84.99	(7)	48.05	(5)	31.68	(3)	23.65	(1)	24.92	(2)
3.0	37.97	(4)	87.69	(6)	94.08	(7)	49.86	(5)	32.67	(3)	24.23	(1)	25.25	(2)
3.5	38.18	(4)	95.73	(6)	103.68	(7)	51.16	(5)	33.39	(3)	24.67	(1)	25.52	(2)
4.0	38.30	(4)	102.03	(6)	111.05	(7)	52.06	(5)	33.87	(3)	24.98	(1)	25.70	(2)

Table 8
Rank scores obtained by the models for each α_c and overall ranking.

α_c	Liu–Jordan	Hay–Davies	Perez1	Perez2	Perez3	Perez4	Perez5
0.5	5	7	6	3	1	2	4
1.0	5	6	7	4	3	1	2
1.5	4	6	7	5	3	1	2
2.0	4	6	7	5	3	1	2
2.5	4	6	7	5	3	1	2
3.0	4	6	7	5	3	1	2
3.5	4	6	7	5	3	1	2
4.0	4	6	7	5	3	1	2
Global	4	6	7	5	3	1	2

$$\mathcal{R}_i = \sum_{j=1}^{m!} \frac{n_j v_j(i)}{n}, \tag{10}$$

where $v_j, j = 1, 2, \ldots, m!$ represents all possible rankings of the $m = 7$ models, n_j is the observed frequency of rank j, $n = \sum_{j=1}^{m} n_j$ and $v_j(i)$ is the rank score given to the model i in the ranking j.

Linear ranking results, for each α_c, as well as an overall rank score that takes into account all the proposed scenarios, are shown in Table 8. These results confirm the good overall performance of the Perez4 and Perez5 models, and the superiority of the Perez3 model for α_c of 0.5.

5. Conclusions

A review of models for estimating diffuse irradiance on inclined planes highlighted the necessity of developing suitable models that take into consideration the effect of obstacles in obstructed urban environments. Three diffuse irradiance models (Liu–Jordan, Hay–Davies and Perez) have been modified accordingly by including two proposed view factors to consider the effect of the urban canyon on the diffuse isotropic background irradiance (*SVF*) and on the circumsolar region (*CVF*). As a result, three modified irradiance models —one of them with five variants— have been obtained.

After applying the ISO/CIE standard to radiance measurements in Pamplona, 5,396 sky types have been obtained for estimating the diffuse irradiance reference value. In this case, most skies (56%) have been classified as clear, 19% as intermediate and almost 25% as overcast. It should be noted that a different sky classification, due to other climatic conditions, might affect the results of the evaluation of the modified irradiance models. Therefore, the influence of the

prevailing sky types in a location should be considered in further research, applying the new approach proposed in this paper for the diffuse irradiance.

Values obtained with the modified irradiance models and the irradiance reference values have been compared by calculating the *rRMSE* in a large number of 4,868 scenarios with different geometry and orientation to cover as many real situations as possible in urban environments. A linear ranking of the models shows that Perez4 model (anisotropic 35° circumsolar region half-angle) exhibits the best performance for seven out of eight urban canyon aspect ratios considered, as well as the best overall behavior, followed by Perez5 model (anisotropic 45° circumsolar region half-angle). The isotropic model occupies an intermediate position, whereas the two anisotropic models that consider the circumsolar region a point source receive the lowest ranking. In addition, the *rRMSE* variation for the different geometries remains low in the best models (18–25%), whereas in the models ranking the last positions the errors greatly increase (over 100%) as the aspect ratio of the urban canyon increases.

In conclusion, the importance of the circumsolar component has been evidenced when estimating the diffuse irradiance on tilted planes in obstructed environments. Specifically, it has been demonstrated how the aperture of the circumsolar region determines the performance of the anisotropic models, being the best performers those models considering a greater aperture angle (35° and 45° circumsolar region half-angle). It has also been shown that, in such obstructed environments, the isotropic model (which omits the circumsolar component) is preferable to the anisotropic models that consider a point source circumsolar region.

Declaration of competing interest

The authors declare that they have no known competing financial interests or personal relationships that could have appeared to influence the work reported in this paper.

Acknowledgments

This work was performed in the framework of the IRILURREFLEX project (ENE2017-86974-R), financed by the Spanish State Research Agency (Agencia Estatal de Investigación, AEI) and the European Regional Development Fund (Fondo Europeo de Desarrollo Regional, FEDER).

Appendix A. Calculation of the projection of sky radiance distribution relative to zenith onto a tilted plane

For a given ISO/CIE model, the projection of the relative radiance of each sky element onto a tilted plane can be obtained by the procedure outlined below and detailed in Fig. A.1. It should be noted that in order to apply the ISO/CIE model, it is necessary to know the spherical coordinates of that element referred to an horizontal plane, i.e., its zenith angle (θ_i) and azimuth angle relative to the south of the place (γ_i). It is also necessary to determine the angular distance between the sky element and the sun (χ_i), which can be obtained from the former and from the spherical coordinates of the sun (θ_z, γ_s). Therefore, the procedure focus on the coordinate transformations that must be applied to the coordinates on the tilted plane (θ'_i, γ'_i) assigned to each sky element after the orthographic projection.

1. On the tilted plane of interest, a square grid is located, with dimensions in accordance to the number of elements in which the hemisphere above the plane is discretized.
2. For the centroid of each grid element, the zenith angle relative to the normal of the tilted plane (θ'_i) and the azimuth angle (γ'_i) relative to the plane azimuth (γ_p) is calculated using the orthographic projection given by Equation (A.1) that relates the projected distance between the centroid of a cell element and the center of the grid (r_i) with θ'_i.

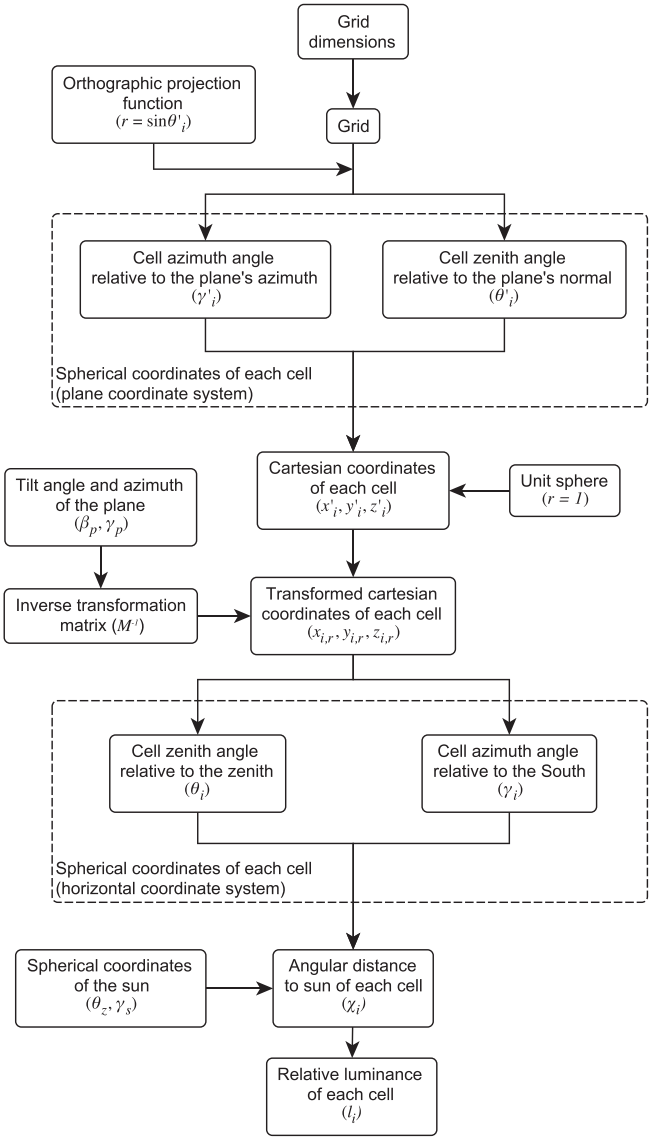

Fig. A.1. Procedure for the calculation of the projection of the sky radiance distribution relative to the zenith onto a tilted plane.

$$r_i = sin(\theta'_i). \tag{A.1}$$

3. For each grid element, the spherical coordinates relative to the inclined plane (θ'_i, γ'_i) are transformed to their corresponding Cartesian coordinates (x'_i, y'_i, z'_i) in the inclined plane, using a unit-radius sphere.
4. Cartesian coordinates in the inclined plane (x'_i, y'_i, z'_i) are transformed to local Cartesian coordinates relative to the zenith and the south (x_i, y_i, z_i) using Equation (A.2), where the transformation matrix (M) defined in Equation (A.3) depends on the azimuth (γ_p) and tilt angle (β_p) of the inclined plane.

$$(x_i, y_i, z_i) = (x'_i, y'_i, z'_i) \cdot M. \tag{A.2}$$

$$M = \begin{pmatrix} cos(\beta_p)cos\left(\gamma_p\right) & cos(\beta_p)sin\left(\gamma_p\right) & -sin(\beta_p) \\ -sin\left(\gamma_p\right) & cos\left(\gamma_p\right) & 0 \\ sin(\beta_p)cos\left(\gamma_p\right) & sin(\beta_p)sin\left(\gamma_p\right) & cos(\beta_p) \end{pmatrix} \tag{A.3}$$

5. The spherical coordinates of the centroid of each sky element (θ_i, γ_i) relative to the zenith and the south are determined from (x_i, y_i, z_i) using a unit-radius sphere.
6. The angle between the sun and each sky element (χ_i) is calculated from the spherical coordinates of each sky element (θ_i, γ_i) and the sun (θ_z, γ_s).
7. For a given ISO/CIE standard sky type, the sky radiance relative to the zenith radiance (l_i) projected onto the grid sky element i is calculated according to Equation (A.4), defined in the ISO 15469:2004(E)/CIE S 011/E:2003 [71] standard.

$$l_i(\theta_i, \gamma_i) = \frac{L_i(\theta_i, \gamma_i)}{L_z} = \frac{f(\chi_i)g(\theta_i)}{f(\theta_z)g(0)}, \tag{A.4}$$

where L_i is the radiance of a sky element i, L_z is the zenith radiance, g is the gradation function, Equation (A.5), and f is the indicatrix function, Equation (A.6). The coefficients (a, b, c, d, e) in Equations (A.5) and (A.6) depend on the standard sky type.

$$\begin{aligned} g(\theta_i) &= 1 + a\exp\left(\frac{b}{\cos\theta_i}\right), \\ g(0) &= 1 + a\exp(b) \end{aligned} \tag{A.5}$$

$$\begin{aligned} f(\chi_i) &= 1 + c\left[\exp(d\chi_i) - \exp\left(d\frac{\pi}{2}\right)\right] + e\cos^2\chi_i, \\ f(\theta_z) &= 1 + c\left[\exp(d\theta_z) - \exp\left(d\frac{\pi}{2}\right)\right] + e\cos^2\theta_z. \end{aligned} \tag{A.6}$$

Note that the procedure detailed in this Appendix is intended for application in the northern hemisphere. Thus, azimuths are measured from due south, increasing towards south-west. That is, azimuth values are negative before solar noon and positive after solar noon. For application in the southern hemisphere, azimuths should be measured from due north, increasing towards the north-west. As in the case of the southern hemisphere, azimuth values will be negative before solar noon and positive after solar noon. The transformation matrix defined in Equation (A.3) is equally applicable in the southern hemisphere, according to the described criterion.

Appendix B. Calculation of sky view factor and circumsolar view factor under obstructed environments

In the absence of obstacles, the *SVF* can be calculated by Equation (B.1) according to the proposal of Liu and Jordan [2], which coincides with that proposed by Kondratyev and Manolova [79] and was originally derived by Moon and Spencer [80].

$$SVF = \frac{G_{d,T}}{G_d} = \frac{1 + \cos\beta_p}{2}. \tag{B.1}$$

In the presence of obstacles, only the visible part of the sky must be considered in the calculation of the *SVF*. Several expresions for the *SVF* can be found in the literature, such as the proposal of Böhner and Antonić [81], an adaptation of the original expression of Dozier and Frew [82]. In the present work however, using a different approach, the *SVF* is calculated by comparing the projections of the sky vault onto the horizontal plane and onto the tilted plane, according to the following procedure.

1. A square grid is placed on the tilted plane of interest, as in step 1 of the procedure described in Appendix A.
2. Using the orthographic projection, the spherical coordinates (θ_i, γ_i) relative to the zenith and south are determined for the centroid of each sky element of the grid, as in step 2 of the procedure described in Appendix A. As an example of application, Fig. B.1b shows the projection of the sky onto a plane with an inclination of 60°.
3. The urban canyon is projected onto the inclined plane, discarding the part of the sky hidden due to the canyon topography. The gray-shaded area in Fig. B.1c corresponds to the projection of an urban canyon with $\alpha_c = 1$ onto the same tilted plane cited in the previous point.
4. The total number of sky elements visible from the plane of interest is computed ($n_{s,T}$).
5. The same procedure is carried out considering this time a horizontal plane free of obstacles, now defining the total number of sky elements visible in this situation ($n_{s,h}$), as seen in Fig. B.1a.
6. The *SVF* is calculated as

$$SVF = \frac{n_{s,T}}{n_{s,h}}. \tag{B.2}$$

As an example, the *SVF* calculated for a particular inclined plane and urban canyon is shown in Fig. B.1.

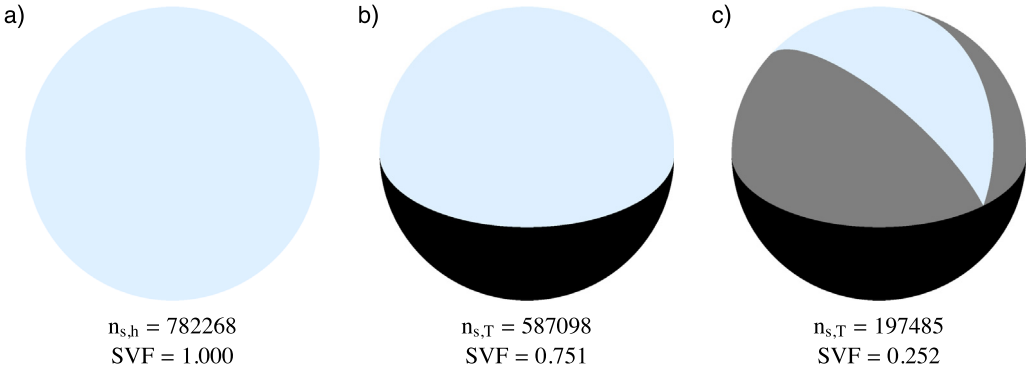

Fig. B.1. Orthographic projection of the sky on (a) a horizontal plane, (b) an obstacle-free plane tilted 60°, and (c) on the same tilted plane located in an urban canyon with $\alpha_c = 1$ and $\gamma_c = 45°$. The black-shaded area corresponds to the part of the ground visible as a consequence of the inclination of the plane. The gray-shaded area corresponds to the projection of the urban canyon on the tilted plane.

The *SVF* is a static parameter, in the sense that it is fixed solely by the plane position and canyon geometry. In contrast, the *CFV* is a dynamic parameter whose value further depends on the position of the sun and on sky conditions. For the calculation of the *CFV*, we propose a procedure analogous to that used for the *SVF*, but restricted to the sky area corresponding to the circumsolar region of interest.

1. The grid on the tilted plane is defined and the spherical coordinates (θ_i, γ_i) relative to the zenith and south, as well as the angular distance to the sun (χ_i) are obtained, following steps 1–6 of the procedure described in Appendix A.
2. All grid sky elements whose angular distance from the sun (χ_i) exceeds the aperture angle of the circumsolar region of interest are discarded. In this study, a range of aperture angles was considered. Fig. B.2b shows an example of the projection of a 25° half-angle circumsolar region onto a 60° tilted plane.
3. The urban canyon is projected on the tilted plane. Grid cells corresponding to the part of the circumsolar region obstructed by the canyon are discarded (see Fig. B.2c).
4. The total number of cells still active, i.e. the total number of elements of the circumsolar region visible from the plane of interest, is computed ($n_{c,T}$).
5. The same procedure is carried out considering an obstacle-free horizontal plane, thus obtaining the number of sky elements included in the circumsolar region visible in this situation ($n_{c,h}$) (see Fig. B.2a).
6. The *CVF* is calculated as

$$CVF = \frac{n_{c,T}}{n_{c,h}}. \tag{B.3}$$

As an example, the *CVF* calculated for a particular inclined plane and urban canyon is shown in Fig. B.2

References

[1] T. Muneer, C.A. Gueymard, H. Kambezidis, Solar Radiation and Daylight Models, Elsevier, 2004, https://doi.org/10.1016/B978-075065974-1/50011-5.
[2] B.Y. Liu, R.C. Jordan, Daily insolation on surfaces tilted towards equator, ASHRAE J. 10 (1961) 53–59.
[3] P.S. Koronakis, On the choice of the angle of tilt for south facing solar collectors in the Athens basin area, Sol. Energy 36 (1986) 217–225, https://doi.org/10.1016/0038-092X(86)90137-4.
[4] Y. Tian, R. Davies-Colley, P. Gong, B. Thorrold, Estimating solar radiation on slopes of arbitrary aspect, Agric. For. Meteorol. 109 (2001) 67–74, https://doi.org/10.1016/S0168-1923(01)00245-3.
[5] V. Badescu, 3D isotropic approximation for solar diffuse irradiance on tilted surfaces, Renew. Energy 26 (2002) 221–233, https://doi.org/10.1016/S0960-1481(01)00123-9.
[6] R.C. Temps, K. Coulson, Solar radiation incident upon slopes of different orientations, Sol. Energy 19 (1977) 179–184, https://doi.org/10.1016/0038-092X(77)90056-1.
[7] J. Bugler, The determination of hourly insolation on an inclined plane using a diffuse irradiance model based on hourly measured global horizontal insolation, Sol. Energy 19 (1977) 477–491, https://doi.org/10.1016/0038-092X(77)90103-7.
[8] T. Klucher, Evaluation of models to predict insolation on tilted surfaces, Sol. Energy 23 (1979) 111–114, https://doi.org/10.1016/0038-092X(79)90110-5.
[9] M.D. Steven, M.H. Unsworth, The diffuse solar irradiance of slopes under cloudless skies, Q. J. R. Meteorol. Soc. 105 (1979) 593–602, https://doi.org/10.1002/qj.49710544507.
[10] J. Hay, J. Davies, Calculation of the solar radiation incident on an inclined surface. Proceedings of the First Canadian Solar Radiation Data Workshop, Ministry of Supply and Services, Toronto, Canada, 1980, pp. 59–72.
[11] C.J. Willmott, On the climatic optimization of the tilt and azimuth of flat-plate solar collectors, Sol. Energy 28 (1982) 205–216, https://doi.org/10.1016/0038-092X(82)90159-1.
[12] C. Ma, M. Iqbal, Statistical comparison of models for estimating solar radiation on inclined surgaces, Sol. Energy 31 (1983) 313–317, https://doi.org/10.1016/0038-092X(83)90019-1.
[13] A. Skartveit, J.A. Olseth, J. Asle Olseth, Modelling slope irradiance at high latitudes, Sol. Energy 36 (1986) 333–344, https://doi.org/10.1016/0038-092X(86)90151-9.
[14] C.A. Gueymard, Radiation on tilted planes: a physical model adaptable to any computational time-step, in: Proceedings of INTERSOL85, Pergamon Press, Elmsford, NY, 1986, pp. 2463–2467. Pergamon Press.
[15] C.A. Gueymard, An anisotropic solar irradiance model for tilted surfaces and its comparison with selected engineering algorithms, Sol. Energy 38 (1987) 367–386, https://doi.org/10.1016/0038-092X(87)90009-0.
[16] R. Perez, R. Seals, P. Ineichen, R. Stewart, D. Menicucci, A new simplified version of the perez diffuse irradiance model for tilted surfaces, Sol. Energy 39 (1987) 221–231, https://doi.org/10.1016/S0038-092X(87)80031-2.
[17] R. Perez, P. Ineichen, R. Seals, J.J. Michalsky, R. Stewart, Modeling daylight availability and irradiance components from direct and global irradiance, Sol.

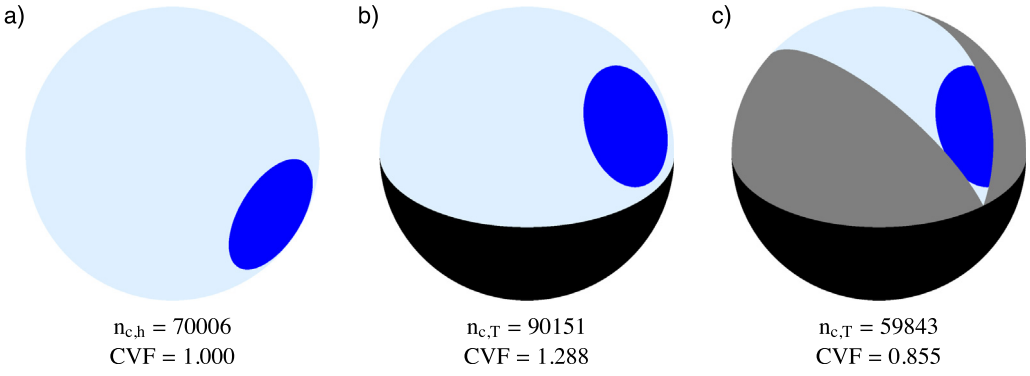

Fig. B.2. Orthographic projection of the circumsolar region on (a) a horizontal plane, (b) an obstacle-free plane tilted 60°, and (c) on the same tilted plane located in an urban canyon with an α_c of 1 and a γ_c of 45°. The represented 25° half-angle circumsolar region is centered at the sun's position ($\theta_z = 60°$, $\gamma_s = -45°$). The black-shaded area corresponds to the visible part of the ground as a consequence of the inclination of the plane. The gray-shaded area corresponds to the projection of the urban canyon onto the tilted plane.

Energy 44 (1990) 271–289, https://doi.org/10.1016/0038-092X(90)90055-H.
[18] G.S. Saluja, T. Muneer, An anisotropic model for inclined surface solar irradiation, Proc. IME C J. Mech. Eng. Sci. 201 (1987) 11–20, https://doi.org/10.1243/PIME_PROC_1987_201_082_02.
[19] D. Reindl, W. Beckman, J. Duffie, Evaluation of hourly tilted surface radiation models, Sol. Energy 45 (1990) 9–17, https://doi.org/10.1016/0038-092X(90)90061-G.
[20] T. Muneer, Solar Radiation Modelling for the United Kingdom, Ph.D. Thesis, Council for National Academic Awards, 1987.
[21] T. Muneer, Solar radiation model for Europe, Build. Serv. Eng. Technol. 11 (1990) 153–163, https://doi.org/10.1177/014362449001100405.
[22] J. Remund, Chain of algorithms to compute hourly radiation data on inclined planes used in meteonorm. Modeling Solar Radiation at the Earth's Surface: Recent Advances, Springer Berlin Heidelberg, 2008, pp. 393–409, https://doi.org/10.1007/978-3-540-77455-6_15.
[23] K. Soga, H. Akasaka, H. Nimiya, A comparison of methods to estimate hourly total irradiation on tilted surfaces from hourly global irradiation on a horizontal surface. Proceedings of Sixth International Conference Building Simulation, Kyoto, Japan, 1999, pp. 635–642.
[24] B.Y. Liu, R.C. Jordan, The long-term average performance of flat-plate solar-energy collectors: with design data for the U.S., its outlying possessions and Canada, Sol. Energy 7 (1963) 53–74, https://doi.org/10.1016/0038-092X(63)90006-9.
[25] J. Hay, Study of short wave radiation on non-horizontal surfaces, For. Rep. (1979), 79-12, Technical Report, Atmospheric Environment Service, Downsview, Ontario.
[26] A. Skartveit, J.A. Olseth, A model for the diffuse fraction of hourly global radiation, Sol. Energy 38 (1987) 271–274, https://doi.org/10.1016/0038-092X(87)90049-1.
[27] H. Akasaka, S. Kuroki, Y. Inamura, H. Nimiya, Measurement and development of estimation formulas for circumsolar and diffuse solar radiation, J. Archit..Plann.Environ.Eng.(Transactions of AIJ) 405 (1989) 19–28, https://doi.org/10.3130/aijax.405.0_19 (in Japanese).
[28] H. Akasaka, S. Kuroki, Models of circumsolar radiation and diffuse sky radiation including cloudy sky, Proceedings of the Biennial Congress of the International Solar Energy Society (1991) 933–938. Denver, 1991-8 1.
[29] G. Notton, P. Poggi, C. Cristofari, Predicting hourly solar irradiations on inclined surfaces based on the horizontal measurements: performances of the association of well-known mathematical models, Energy Convers. Manag. 47 (2006) 1816–1829, https://doi.org/10.1016/J.ENCONMAN.2005.10.009.
[30] J. Jiménez, Y. Castro, National Assembly of Geophysics and Geodesy II, 1981, p. 805.
[31] R. Perez, R. Stewart, C. Arbogast, R. Seals, J. Scott, An anisotropic hourly diffuse radiation model for sloping surfaces: description, performance validation, site dependency evaluation, Sol. Energy 36 (1986) 481–497, https://doi.org/10.1016/0038-092X(86)90013-7.
[32] M. Iqbal, An Introduction to Solar Radiation, Elsevier, 1983, https://doi.org/10.1016/B978-0-12-373750-2.X5001-0.
[33] C.A. Gueymard, From global horizontal to global tilted irradiance: how accurate are solar energy engineering predictions in practice?, in: American Solar Energy Society, Solar 2008 Conference American Solar Energy Society, San Diego, CA, 2008.
[34] C.A. Gueymard, Erratum, Solar Energy 40 (1988) 175, https://doi.org/10.1016/0038-092X(88)90087-4.
[35] J. Hay, Calculation of monthly mean solar radiation for horizontal and inclined surfaces, Sol. Energy 23 (1979) 301–307, https://doi.org/10.1016/0038-092X(79)90123-3.
[36] J. Duffie, W. Beckman, Solar Engineering of Thermal Processes, second ed., John Wiley and Sons, New York: USA, 1991.
[37] ASHRAE, Handbook of Fundamentals, American Society of Heating, Refrigerating and Air-Conditioning Engineers, Atlanta (GA, USA), 2005.
[38] A.M. Noorian, I. Moradi, G.A. Kamali, Evaluation of 12 models to estimate hourly diffuse irradiation on inclined surfaces, Renew. Energy 33 (2008) 1406–1412, https://doi.org/10.1016/J.RENENE.2007.06.027.
[39] M.D. Steven, M.H. Unsworth, The angular distribution and interception of diffuse solar radiation below overcast skies, Q. J. R. Meteorol. Soc. 106 (1980) 57–61, https://doi.org/10.1002/qj.49710644705.
[40] E.G. Evseev, A.I. Kudish, The assessment of different models to predict the global solar radiation on a surface tilted to the south, Sol. Energy 83 (2009) 377–388, https://doi.org/10.1016/J.SOLENER.2008.08.010.
[41] T. Muneer, Solar Radiation and Daylight Models for the Energy Efficient Design of Buildings, vol. 26, Arquitectural Press, 1997.
[42] S.A. Khalil, A. Shaffie, A comparative study of total, direct and diffuse solar irradiance by using different models on horizontal and inclined surfaces for Cairo, Egypt, Renew. Sustain. Energy Rev. 27 (2013) 853–863, https://doi.org/10.1016/J.RSER.2013.06.038.
[43] C. Demain, M. Journée, C. Bertrand, Evaluation of different models to estimate the global solar radiation on inclined surfaces, Renew. Energy 50 (2013) 710–721, https://doi.org/10.1016/J.RENENE.2012.07.031.
[44] W. Yao, Z. Li, Q. Zhao, Y. Lu, R. Lu, A new anisotropic diffuse radiation model, Energy Convers. Manag. 95 (2015) 304–313, https://doi.org/10.1016/J.ENCONMAN.2015.01.016.
[45] R. Mubarak, M. Hofmann, S. Riechelmann, G. Seckmeyer, Comparison of modelled and measured tilted solar irradiance for photovoltaic applications, Energies 10 (2017) 1688, https://doi.org/10.3390/en10111688.
[46] M. de Simón-Martín, C. Alonso-Tristán, M. Díez-Mediavilla, Diffuse solar irradiance estimation on building's façades: review, classification and benchmarking of 30 models under all sky conditions, Renew. Sustain. Energy Rev. 77 (2017) 783–802, https://doi.org/10.1016/j.rser.2017.04.034.
[47] C.A. Gueymard, On the correct use of the Gueymard diffuse radiation model for tilted surfaces, Energy Convers. Manag. 101 (2015) 787–788, https://doi.org/10.1016/j.enconman.2015.05.046.
[48] M. Lockmanhekim, Procedure for determining heating and cooling loads for computerized energy calculations. Algorithms for Building Heat Transfer Subroutines, Task Group on Energy Requirements for Heating and Cooling, American Society of Heating, Refrigerating and Air-Conditioning Engineers, New York, NY, 1971.
[49] J.E. Hay, A revised method for determining the direct and diffuse components of the total short-wave radiation, Atmosphere 14 (1976) 278–287, https://doi.org/10.1080/00046973.1976.9648423.
[50] J.J. Hirsch, DOE-2 Building Energy Use and Cost Analysis Tool: DOE-2.3, 2020. URL: https://doe2.com/DOE2/index.html.
[51] T. Muneer, Solar irradiance and illuminance models for Japan I: sloped surfaces, Light. Res. Technol. 27 (1995) 209–222, https://doi.org/10.1177/14771535950270040601.
[52] M. Díez-Mediavilla, Medida y modelización de radiación solar difusa sobre plano inclinado, Ph.D. thesis, Universidad de Valladolid, 2001.
[53] F. Olmo, J. Vida, I. Foyo, Y. Castro-Diez, L. Alados-Arboledas, Prediction of global irradiance on inclined surfaces from horizontal global irradiance, Energy 24 (1999) 689–704, https://doi.org/10.1016/S0360-5442(99)00025-0.
[54] E. Ruiz, A. Soler, L. Robledo, Comparison of the Olmo model with global irradiance measurements on vertical surfaces at Madrid, Energy 27 (2002) 975–986, https://doi.org/10.1016/S0360-5442(02)00013-0.
[55] E.G. Evseev, A.I. Kudish, An assessment of a revised Olmo et al. model to predict solar global radiation on a tilted surface at Beer Sheva, Israel, Renew. Energy 34 (2009) 112–119, https://doi.org/10.1016/j.renene.2008.04.012.
[56] I. García, J.L. Torres, M. de Blas, C. Sáenz, B. Hernández, R. Illanes Muñoz, Evaluación comparativa de 19 modelos de estimación de irradiancia difusa sobre planos inclinados dependiendo del tipo de cielo estándar ISO/CIE, 2020, pp. 869–877, https://doi.org/10.34637/cies2020.1.6103. As Energias Renováveis na Transição Energética: Livro de Comunicações do XVII Congresso Ibérico e XIII Congresso Ibero-americano de Energia Solar, Lisbon, Portugal (in Spanish).
[57] V. Costanzo, R. Yao, E. Essah, L. Shao, M. Shahrestani, A. Oliveira, M. Araz, A. Hepbasli, E. Biyik, A method of strategic evaluation of energy performance of Building Integrated Photovoltaic in the urban context, J. Clean. Prod. 184 (2018) 82–91, https://doi.org/10.1016/j.jclepro.2018.02.139.
[58] T.R. Oke, Canyon geometry and the nocturnal urban heat island: comparison of scale model and field observations, J. Climatol. 1 (1981) 237–254, https://doi.org/10.1002/joc.3370010304.
[59] G.T. Johnson, I.D. Watson, The determination of view-factors in urban canyons, J. Clim. Appl. Meteorol. 23 (1984) 329–335, 10.1175/1520-0450(1984)023<0329:TDOVFI>2.0.CO;2.
[60] P. Redweik, C. Catita, M. Brito, Solar energy potential on roofs and facades in an urban landscape, Sol. Energy 97 (2013) 332–341, https://doi.org/10.1016/J.SOLENER.2013.08.036.
[61] C. Ratti, P. Richens, Raster analysis of urban form, Environ. Plann. Plann. Des. 31 (2004) 297–309, https://doi.org/10.1068/b2665.
[62] L. Kómar, M. Kocifaj, Uncertainty of daylight illuminance on vertical building façades when determined from sky scanner data: a numerical study, Sol. Energy 110 (2014) 15–21, https://doi.org/10.1016/J.SOLENER.2014.09.010.
[63] A.M. Gracia, J.L.J. Torres, M. De Blas, A. García, R. Perez, Comparison of four luminance and radiance angular distribution models for radiance estimation, Sol. Energy 85 (2011) 2202–2216, https://doi.org/10.1016/j.solener.2011.06.005.
[64] E. Vartiainen, A new approach to estimating the diffuse irradiance on inclined surfaces, Renew. Energy 20 (2000) 45–64, https://doi.org/10.1016/S0960-1481(99)00086-5.
[65] R. Perez, R. Seals, J.J. Michalsky, All-weather model for sky luminance distribution—preliminary configuration and validation, Sol. Energy 50 (1993) 235–245, https://doi.org/10.1016/0038-092X(93)90017-I.
[66] S.M. Ivanova, Estimation of background diffuse irradiance on orthogonal surfaces under partially obstructed anisotropic sky. Part I – vertical surfaces, Sol. Energy 95 (2013) 376–391, https://doi.org/10.1016/j.solener.2013.01.021.
[67] P. Clarke, T. Muneer, A. Davidson, J. Kubie, Models for the estimation of building integrated photovoltaic systems in urban environments, Proc. IME J. Power Energy 222 (2008) 61–67, https://doi.org/10.1243/09576509JPE474.
[68] S.M. Ivanova, C.A. Gueymard, Simulation and applications of cumulative anisotropic sky radiance patterns, Sol. Energy 178 (2019) 278–294, https://doi.org/10.1016/J.SOLENER.2018.12.026.
[69] N. Igawa, Improving the All Sky Model for the luminance and radiance distributions of the sky, Sol. Energy 105 (2014) 354–372, https://doi.org/10.1016/j.solener.2014.03.020.
[70] M. Nunez, T.R. Oke, The energy balance of an urban canyon, Journal of Applied Meteorology and Climatology 16 (1977) 11–19, 10.1175/1520-0450(1977)016<0011:TEBOAU>2.0.CO;2.
[71] ISO 15469:2004(E)/CIE S 011/E:2003, Spatial Distribution of Daylight – CIE Standard General Sky, Technical Report, ISO, Geneva, 2004. Vienna: CIE.
[72] CIE, Guide to recommended practice of daylight measurement, CIE Central Bureau, Vienna, Austria, 1994. Technical Report CIE 108:1994, Technical

Report, CIE.
[73] C. Hoyer-Klick, D. Dumortier, A. Tsvetkov, J. Polo, J.L. Torres, C. Kurz, P. Ineichen, D 1.1.2 Existing Ground Data Sets. Management and Exploitation of Solar Resource Knowledge. CA – Contract No. 038665, Technical Report, Management and Exploitation of Solar Resource Knowledge, CA – Contract No, 2008, 38665.
[74] D.H. Li, T.N. Lam, K.L. Cheung, H.L. Tang, An Analysis of Luminous Efficacies under the CIE Standard Skies, Renewable Energy, 2008, https://doi.org/10.1016/j.renene.2008.02.004.
[75] I. García, M. de Blas, J.L. Torres, The sky characterization according to the CIE Standard General Sky: comparative analysis of three classification methods, Sol. Energy 196 (2020) 468–483, https://doi.org/10.1016/j.solener.2019.12.039.
[76] A. Bartzokas, H. Kambezidis, S. Darula, R. Kittler, Comparison between winter and summer sky-luminance distribution in central europe and in the eastern mediterranean, J. Atmos. Sol. Terr. Phys. 67 (2005) 709–718, https://doi.org/10.1016/J.JASTP.2004.12.008.
[77] D. Yang, Solar radiation on inclined surfaces: corrections and benchmarks, Sol. Energy 136 (2016) 288–302, https://doi.org/10.1016/J.SOLENER.2016.06.062.
[78] M. Alvo, P.L.H. Yu, Exploratory analysis of ranking data. Statistical Methods for Ranking Data, Springer, New York, New York, NY, 2014, pp. 7–21, https://doi.org/10.1007/978-1-4939-1471-5_2.
[79] K. Kondratyev, M. Manolova, The radiation balance of slopes, Sol. Energy 4 (1960) 14–19, https://doi.org/10.1016/0038-092X(60)90041-4.
[80] P. Moon, D. Spencer, Illumination from a non-uniform sky, Trans. Illum. Eng. Soc. 37 (1942) 707–726.
[81] J. Böhner, O. Antonić, Geomorphometry - concepts, software, applications, Dev. Soil Sci. 33 (2009), https://doi.org/10.1016/S0166-2481(08)00008-1. Elsevier.
[82] J. Dozier, J. Frew, Rapid calculation of terrain parameters for radiation modeling from digital elevation data, IEEE Trans. Geosci. Rem. Sens. 28 (1990) 963–969, https://doi.org/10.1109/36.58986.